Identification of elastic properties of human patellae using micro finite element analysis

A. Latypova[1], G. Maquer[2], Elankumaran. K.[3], D. Pahr[3], P. Zysset[2], D.P. Pioletti[1], A. Terrier[1]

1 Laboratory of Biomechanical Orthopedics, EPFL, Lausanne, Switzerland
2 Institute for Surgical Technology and Biomechanics, UniBe, Bern, Switzerland
3 Institute of Lightweight Design and Structural Biomechanics, TUWien, Vienna, Austria

Corresponding author
Alexandre Terrier, PhD
Laboratory of Biomechanical Orthopedics
Ecole Polytechnique Fédérale de Lausanne
Station 19
1015 Lausanne
Switzerland
Phone: +41 21 693 9994
Fax: +41 21 693 8660
Email: alexandre.terrier@epfl.ch

Abstract word count: 189

Main text word count: 2021

Keywords: Patella; Bone Mechanics; Trabecular Anisotropy; Finite Element Analysis

Conflict of interest: None of the authors has any conflict of interest.

Acknowledgments: This study was supported by the “Fondation de soutien à la recherche dans le domaine de l’orthopédie-traumatologie”.

1. Introduction

Currently, the existing homogenized finite element (hFE) models of patella rely on material laws identified not on the patellar bone, but, for example, femur or vertebra (Fitzpatrick et al., 2011; Ho et al., 2014; Takahashi et al., 2012). Furthermore, the anisotropy of the trabecular bone, shown to be crucial for predicting its elastic properties on various anatomical sites (Maquer et al., 2015), is completely overlooked.

Abrupt changes of main trabecular orientations (Raux et al., 1975) and the small size of the patella make it difficult to extract samples of appropriate dimensions for biomechanical testing and complicate accurate experimental measurements (Lammentausta et al., 2006). In such cases, micro finite element (μFE) modeling based on high-resolution μCT reconstruction is a common alternative to *in vitro* mechanical testing (Pistoia et al., 2002; van Rietbergen and Ito, 2015; Wolfram et al., 2010). This method avoids preparation- and damage-related artefacts and restriction regarding the number of load-cases used to assess the elastic constants. Besides, the influence of any bony feature observable on μCT images can be reflected in the analysis.

Therefore, the aim of this study was to identify and validate elastic constants of the patellar bone specifically. The anisotropic constitutive law based on morphology-elasticity relationship and alternative isotropic law based on bone volume fraction were considered. Identification of homogenized models was performed by means of μFE simulated mechanical tests of μCT scanned cadaveric patellae. To validate the identified parameters, predictions of hFE models build from μCT and CT scans of cadaveric patellar sections were compared to μFE predictions of the same patellae.

2. Materials and methods

2.1 µCT and CT imaging

Twenty fresh-frozen cadaveric patellae (12 male, 8 female; age range 15-93, mean age 67 ± 17) after thawing at room temperature overnight and bubble removal, were scanned with a µCT (Skyscan 1076, Bruker microCT, Kontich, Belgium) in a saline soaked gauze with the following scanning settings: 18.3 µm resolution, 80 kV/120 µA, 540 ms exposure time, 1 mm aluminum filter, 0.2 degree rotation step. The patellae were then CT scanned (Discovery 110 CT750 HD, GE Healthcare, Milwaukee, USA) with a resolution of $0.39 \times 0.39 \times 0.625$ mm^3. The µCT images were downscaled to 36.6 µm resolution and segmented using a single level threshold algorithm (Ridler and Calvard, 1978). Image pre-processing was done in Medtool (www.dr-pahr.at).

2.2 Identification of the material laws

The following constitutive law was considered (Zysset, 2003; Zysset and Curnier, 1995):

$$E_i = E_0\rho^k(m_i^2)^l,\ \frac{E_i}{\nu_{ij}} = \frac{E_0}{\nu_0}\rho^k(m_i m_j)^l,\ G_{ij} = G_0\rho^k(m_i m_j)^l,\ \forall i \neq j = 1,2,3\ , \quad (1)$$

where E_i, ν_{ij}, and G_{ij} are engineering constants, E_0, ν_0, G_0, k, l are model parameters, ρ is the bone volume fraction, and m_i are the normalized eigenvalues of the second-order fabric tensor $\boldsymbol{M}$ (Cowin, 1985). The isotropic case was based on the same relationship with $\boldsymbol{M}$ equal to the identity tensor $\boldsymbol{I}$.

To identify the model parameters, simple mechanical tests were conducted via µFE on 200 trabecular cubes (5.3 mm side length), virtually extracted from µCT scans of all patellae. Cubes were visually checked to have relatively homogeneous bone distribution within volume, without

abrupt change in trabecular direction, and a sufficient amount of trabecular on the sides to provide proper load transition (Figure 1). Bone volume fraction (*ρ),* defined as bone volume over the total tissue volume, fabric tensor $\boldsymbol{M}$, established through mean intercept length (MIL) (Laib et al., 1998; Whitehouse, 1974), and the degree of anisotropy (DA), defined as a ratio between maximum and minimum eigenvalues of fabric tensor (Hildebrand et al., 1999), were measured for each cube. All cubes were converted into µFE models with linear hexahedral elements (about 9 million degrees of freedom) following a linear elastic law (E = 12 GPa, $\boldsymbol{\nu}$ = 0.3) for bone tissue (Wolfram et al., 2010). Three compression and three shear load cases were applied to each cube under kinematic uniform boundary conditions (KUBC) (Pahr and Zysset, 2008). The full stiffness tensor ($\mathbf{C}_{\mu FE\_aniso}$) of each cube was obtained by averaging µFE local strain and stress predictions. The orthotropic approximation ($\mathbf{C}_{\mu FE\_ortho}$) of the stiffness tensor was considered for further analysis. The norm error associated with this assumption was calculated by

$$NE_{aniso-ortho} = \frac{\|C_{\mu FE\_aniso} - C_{\mu FE\_ortho}\|}{\|C_{\mu FE\_aniso}\|} \quad (2)$$

Model parameters were identified by fitting the material law (1) to components of µFE stiffness tensor, using multi linear regressions in logarithmic scale. The same procedure was repeated for the isotropic model. Pre- and post-processing were done in Medtool, and µFE simulations were performed using ParFE (parfe.sourceforge.net).

2.3 Validation of the material laws

To validate the material laws, µFE and hFE predictions of cuboid sections ($15 \times 22 \times 16$ mm^3 (± 8mm^3)) of 18 out of 20 patellae were compared. One patella was excluded due to bone defects (probably metastases), and for one section µFE simulations did not converge. The sections were extracted from µCT scans by cropping the superior-inferior and medial-lateral sides, and

embedding the anterior and posterior sides (Figure 1). The embedding was modeled as linear elastic material (E = 1400 MPa, $\boldsymbol{\nu}$ = 0.3). Three tension and three shear KUBC load cases were simulated. Each µFE model had approximately 350 million degrees of freedom. The µFE simulations were performed using ParOSol (bitbucket.org/Elankumaran/parosol-tu-wien). The hFE model meshes were created based on the same cropped µCT images downscaled to 0.54 mm voxel size. Each voxel was converted to a linear hexahedral element. Material properties of each bone element of the anisotropic model were automatically assigned by Medtool from original segmented µCT images, according to bone volume fraction and fabric (MIL) measured in 5.3-mm-diameter spherical volumes positioned in nodes of the µCT 2.0-mm-side-length background grid (Pahr and Zysset, 2009). In case of the isotropic model, the bone volume fraction was estimated from Hounsfield units (HU) of CT calibrated images (Latypova et al., 2016):

$$\rho = 1.0614 \times BMD - 0.0573,\ BMD = (HU-1)/1510 \quad (3)$$

The same parameters for background grid and spherical volumes were used. Each hFE model had approximately 9×10^4 degrees of freedom. The hFE simulations were performed with Abaqus/Standard (Simulia, Providence, RI, USA).

To compare global µFE and hFE predictions, the stiffness matrices of the whole sections were calculated through the averaged strain and stress tensors and the orthotropic part was considered ($\mathbf{C}_{\mu FE}$ and $\mathbf{C}_{hFE}$). The difference was estimated by

$$NE_{hFE} = \frac{\|C_{\mu FE} - C_{hFE}\|}{\|C_{\mu FE}\|} \quad (4)$$

In addition, the statistical significance between error induced by isotropic and anisotropic assumption was estimated with paired t-test. For local comparison, ten cubic (5.4 mm side) regions of interest (ROI) were extracted from each section. The size of the cubes was chosen to be consistent with the homogenization during the identification study. The components of strain

and stress tensors were averaged on these ROIs. Volumetric strain (trE), octahedral shear strain (OctSS), volumetric stress (trS/3), von Mises stress (Mises), and strain energy density (SED) were compared. The hFE predictions were quantified with adjusted correlation coefficient (r^2_{adj}), concordance correlation coefficient (ccc) (Lin, 1989), root mean square error (RMSE) and *p* value. The statistical significance between the correlations was analyzed with Williams formula proposed by (Steiger, 1980). Significance level was set to 95% ($p < 0.05$) for all statistical analyses. The analysis of OctSS, Mises and SED followed a logarithmic transformation. Global stiffness was obtained by post-processing functions of Medtool. Strain and stress tensors in integration points of ROI were extracted from µFE results with Paraview (paraview.org), and with python script (Python 2.6.6) from the hFE results. ROIs were extracted from 10 patellar sections since 8 of 18 sections could not be loaded in Paraview, probably due to large (up to 42 GB) file sizes.

3. Results

The average bone volume fraction ρ of 200 cubes was 0.29 ± 0.11. Eigenvalues of the fabric tensor were $m_1 = 0.77 \pm 0.07$, $m_2 = 0.99 \pm 0.06$, $m_3 = 1.23 \pm 0.09$. DA was 1.62 ± 0.23. The norm error $NE_{aniso\text{-}ortho}$ was 6.15 ± 2.92%. Both anisotropic and isotropic homogenized laws were strongly correlated to the µFE reference (Table 1).

The validation was conducted on 18 sections. Both anisotropic and isotropic hFE showed good match to µFE reference (Table 1). The anisotropic norm error NE_{hFE} was lower (13 ± 5%) than the isotropic one (18 ± 6%). The isotropic norm error was statistically significantly different from anisotropic norm error (p = 0.0009).

Local comparison was conducted on 100 cubic ROIs. The correlations of hFE against μFE for volumetric strain and stress were strong for anisotropic and isotropic models, but better for anisotropic one (Table 1). For OctSS, SED and Mises, anisotropic predictions also provided higher correlation coefficients, slopes of regression line closer to unit and lower RMS errors. The correlations were statistically significantly different ($p<0.001$). The strain and stress distribution of hFE model was visually consistent with μFE reference (Figure 2).

4. Discussion

Currently, literature is lacking validated material law for the patellar bone that can be implemented in hFE models. Such models can be used for numerical predictions of patellar strain in order to better understand patellar pathologies such as fracture after total knee arthroplasty (Fitzpatrick et al., 2011; Fitzpatrick et al., 2013) or anterior knee pain (Ho et al., 2014). In this study we identified and validated anisotropic and isotropic material models for patellar trabecular bone by means of μFE analyses on 20 cadaveric patellae that can be further used in hFE models.

The average bone volume fraction ρ of the extracted cubes was consistent with the reported values (Lammentausta et al., 2006; Raux et al., 1975). The structure of the patellar trabecular was found to be closer to orthotropic rather than isotropic or transverse isotropic. The low error caused by orthotropic approximation confirmed this observation. The average degree of anisotropy was in the range of other anatomical zones (femur, radius, and vertebra) (Gross et al., 2013), but no data for the patellar bone was found for comparison. The identified model parameters were also consistent with the literature (Gross et al., 2013), but higher exponential constants were obtained. It suggests that higher stiffness at low bone volume fraction zones and

lower stiffness at higher bone volume fraction zones will be assigned to the patellar hFE if material parameters from other anatomical sites are used.

For validation of the identified elastic laws, the global stiffness and local strain and stress invariants of the bone sections modeled as hFE was compared to its μFE equivalent. The isotropic hFE was based on CT images since currently it is a gold standard in clinical application. The analyzed invariants were chosen as the common descriptors of bone strain and stress state that can be linked with bone damage. Both models showed highly significant correlation to μFE predictions, however, as expected, accounting for the trabecular fabric improved the correlation of the model against the μFE analyses (Gross et al., 2013; Maquer et al., 2015). Even though the anisotropic model better predicted the μFE global stiffness, it was still found slightly less stiff, possibly due to the lack of explicit cortex modeling (Pahr and Zysset, 2009). The highest variation between μFE and hFE stress predictions was found in cubes with low stress values caused by low bone volume fraction. These finding supports results of a similar study conducted on the proximal femur (Hazrati Marangalou et al., 2012). The correlation of the local strain predictions was lower than those of stress predictions most probably due to the lower variation of strain values.

Several limitations of the study should be mentioned. The identification was conducted on bone cubes using kinematic uniform boundary conditions that tend to overestimate bone effective stiffness (Hazanov and Huet, 1994). The bone tissue was assumed homogeneous and isotropic material, but it was demonstrated previously that heterogeneous tissue mineralization has only a minor effect on apparent trabecular bone elastic properties (Gross et al., 2012). The material model validation with six canonical loading cases of patellar cuboid sections allowed controlled boundary conditions and easy result interpretation (van Rietbergen and Ito, 2015; Zysset et al.,

2013). However, predictions of anisotropic and isotropic models should be further compared for a whole patella under more physiological loading conditions. The importance of modeling anisotropy could be further emphasized in such case.

In conclusion, an anisotropic and an isotropic morphology-elasticity model for patellar trabecular bone were identified and validated. When high-resolution images are available, the anisotropic material parameters can be assigned to hFE models, assuming direct access to bone volume fraction and fabric tensor from images. When only low-resolution images are available, such as clinical CT scans, the isotropic model is a reasonable alternative. The anisotropic model might still be applicable by estimating anisotropy with recently proposed approaches, such as database approach or μCT template registration (Marangalou et al., 2013; Taghizadeh et al., 2016).

References

Cowin, S.C., 1985. The Relationship between the Elasticity Tensor and the Fabric Tensor. Mech Mater 4, 137-147.

Fitzpatrick, C.K., Baldwin, M.A., Ali, A.A., Laz, P.J., Rullkoetter, P.J., 2011. Comparison of patellar bone strain in the natural and implanted knee during simulated deep flexion. Journal of orthopaedic research : official publication of the Orthopaedic Research Society 29, 232-239.

Fitzpatrick, C.K., Kim, R.H., Ali, A.A., Smoger, L.M., Rullkoetter, P.J., 2013. Effects of resection thickness on mechanics of resurfaced patellae. Journal of biomechanics 46, 1568-1575.

Gross, T., Pahr, D.H., Peyrin, F., Zysset, P.K., 2012. Mineral heterogeneity has a minor influence on the apparent elastic properties of human cancellous bone: a SRmuCT-based finite element study. Computer methods in biomechanics and biomedical engineering 15, 1137-1144.

Gross, T., Pahr, D.H., Zysset, P.K., 2013. Morphology-elasticity relationships using decreasing fabric information of human trabecular bone from three major anatomical locations. Biomechanics and modeling in mechanobiology 12, 793-800.

Hazanov, S., Huet, C., 1994. Order Relationships for Boundary-Conditions Effect in Heterogeneous Bodies Smaller Than the Representative Volume. J Mech Phys Solids 42, 1995-2011.

Hazrati Marangalou, J., Ito, K., van Rietbergen, B., 2012. A new approach to determine the accuracy of morphology-elasticity relationships in continuum FE analyses of human proximal femur. Journal of biomechanics 45, 2884-2892.

Hildebrand, T., Laib, A., Muller, R., Dequeker, J., Ruegsegger, P., 1999. Direct three-dimensional morphometric analysis of human cancellous bone: microstructural data from spine, femur, iliac crest, and calcaneus. Journal of bone and mineral research : the official journal of the American Society for Bone and Mineral Research 14, 1167-1174.

Ho, K.Y., Keyak, J.H., Powers, C.M., 2014. Comparison of patella bone strain between females with and without patellofemoral pain: A finite element analysis study. Journal of biomechanics 47, 230-236.

Laib, A., Hauselmann, H.J., Ruegsegger, P., 1998. In vivo high resolution 3D-QCT of the human forearm. Technology and health care : official journal of the European Society for Engineering and Medicine 6, 329-337.

Lammentausta, E., Hakulinen, M.A., Jurvelin, J.S., Nieminen, M.T., 2006. Prediction of mechanical properties of trabecular bone using quantitative MRI. Physics in medicine and biology 51, 6187-6198.

Latypova, A., Arami, A., Becce, F., Jolles-Haeberli, B., Aminian, K., Pioletti, D.P., Terrier, A., 2016. A patient-specific model of total knee arthroplasty to estimate patellar strain: A case study. Clin Biomech (Bristol, Avon) 32, 212-219.

Lin, L.I., 1989. A concordance correlation coefficient to evaluate reproducibility. Biometrics 45, 255-268.

Maquer, G., Musy, S.N., Wandel, J., Gross, T., Zysset, P.K., 2015. Bone Volume Fraction and Fabric Anisotropy Are Better Determinants of Trabecular Bone Stiffness Than Other Morphological Variables. Journal of Bone and Mineral Research 30, 1000-1008.

Marangalou, J.H., Ito, K., Cataldi, M., Taddei, F., van Rietbergen, B., 2013. A novel approach to estimate trabecular bone anisotropy using a database approach. Journal of biomechanics 46, 2356-2362.

Pahr, D.H., Zysset, P.K., 2008. Influence of boundary conditions on computed apparent elastic properties of cancellous bone. Biomechanics and modeling in mechanobiology 7, 463-476.

Pahr, D.H., Zysset, P.K., 2009. A comparison of enhanced continuum FE with micro FE models of human vertebral bodies. Journal of biomechanics 42, 455-462.

Pistoia, W., van Rietbergen, B., Lochmuller, E.M., Lill, C.A., Eckstein, F., Ruegsegger, P., 2002. Estimation of distal radius failure load with micro-finite element analysis models based on three-dimensional peripheral quantitative computed tomography images. Bone 30, 842-848.

Raux, P., Townsend, P.R., Miegel, R., Rose, R.M., Radin, E.L., 1975. Trabecular architecture of the human patella. Journal of biomechanics 8, 1-7.

Ridler, T.W., Calvard, S., 1978. Picture Thresholding Using an Iterative Selection Method. Ieee T Syst Man Cyb 8, 630-632.

Steiger, J.H., 1980. Tests for Comparing Elements of a Correlation Matrix. Psychol Bull 87, 245-251.

Taghizadeh, E., Reyes, M., Zysset, P., Latypova, A., Terrier, A., Buchler, P., 2016. Biomechanical Role of Bone Anisotropy Estimated on Clinical CT Scans by Image Registration. Annals of biomedical engineering.

Takahashi, A., Sano, H., Ohnuma, M., Kashiwaba, M., Chiba, D., Kamimura, M., Sugita, T., Itoi, E., 2012. Patellar morphology and femoral component geometry influence patellofemoral contact stress in total knee arthroplasty without patellar resurfacing. Knee surgery, sports traumatology, arthroscopy : official journal of the ESSKA 20, 1787-1795.

van Rietbergen, B., Ito, K., 2015. A survey of micro-finite element analysis for clinical assessment of bone strength: The first decade. Journal of biomechanics 48, 832-841.

Whitehouse, W.J., 1974. The quantitative morphology of anisotropic trabecular bone. Journal of microscopy 101, 153-168.

Wolfram, U., Wilke, H.J., Zysset, P.K., 2010. Valid micro finite element models of vertebral trabecular bone can be obtained using tissue properties measured with nanoindentation under wet conditions. Journal of biomechanics 43, 1731-1737.

Zysset, P.K., 2003. A review of morphology-elasticity relationships in human trabecular bone: theories and experiments. Journal of biomechanics 36, 1469-1485.

Zysset, P.K., Curnier, A., 1995. An Alternative Model for Anisotropic Elasticity Based on Fabric Tensors. Mech Mater 21, 243-250.

Zysset, P.K., Dall'ara, E., Varga, P., Pahr, D.H., 2013. Finite element analysis for prediction of bone strength. BoneKEy reports 2, 386.

List of Figures and Tables

Table 1. Results of identification and validation studies. Identification includes parameters for anisotropic and isotropic morphology-elasticity models, results of regression analysis. Validation includes regression analysis between components of global stiffness matrices (Glob stiff), local volumetric strain (trE) and stress (trS/3), octahedral shear strain (OctSS), von Mises stress (Mises) and strain energy density (SED) calculated with anisotropic and isotropic hFE models against μFE reference. For OctSS, Mises and SED regression is done in logarithmic space. In the table, the "A" stands for anisotropic and the "I" for isotropic models. In regression, the "x" stands for hFE and the "y" stands for μFE predictions.

Identification										
	E_0 *(MPa)*	v_0	G_0 *(MPa)*	k	l	**Regression**	r^2_{adj}	**ccc**	**RMSE**	**p-value**
A	12723.1	0.24	4224.6	2.1	1.02	y = 0.949x + 0.316	0.95	0.97	0.20	<0.001
I	11035.9	0.26	4395.1	2.13	-	y = 0.838x + 1.000	0.85	0.92	0.32	<0.001
Validation										
Glob stiff	**A**					y = 1.070x - 0.641	0.96	0.96	0.16	<0.001
	I					y = 0.978x + 0.094	0.93	0.96	0.21	<0.001
trS/3	**A**					y = 0.972x + 0.013	0.98	0.98	0.08	<0.001
	I					y = 0.846x + 0.021	0.94	0.96	0.16	<0.001
trE	**A**					$y = 0.961x + 1e^{-5}$	0.98	0.99	$8e^{-5}$	<0.001
	I					$y = 0.962x + 2e^{-5}$	0.96	0.98	$1e^{-4}$	<0.001
OSS	**A**					y = 0.988x - 0.083	0.84	0.91	0.07	<0.001
	I					y = 0.946x - 0.367	0.71	0.84	0.10	<0.001
Mises	**A**					y = 0.913x - 0.001	0.96	0.98	0.19	<0.001
	I					y = 0.792x - 0.112	0.80	0.79	0.33	<0.001
SED	**A**					y = 0.913x - 0.662	0.98	0.98	0.17	<0.001
	I					y = 0.835x - 1.316	0.89	0.86	0.29	<0.001

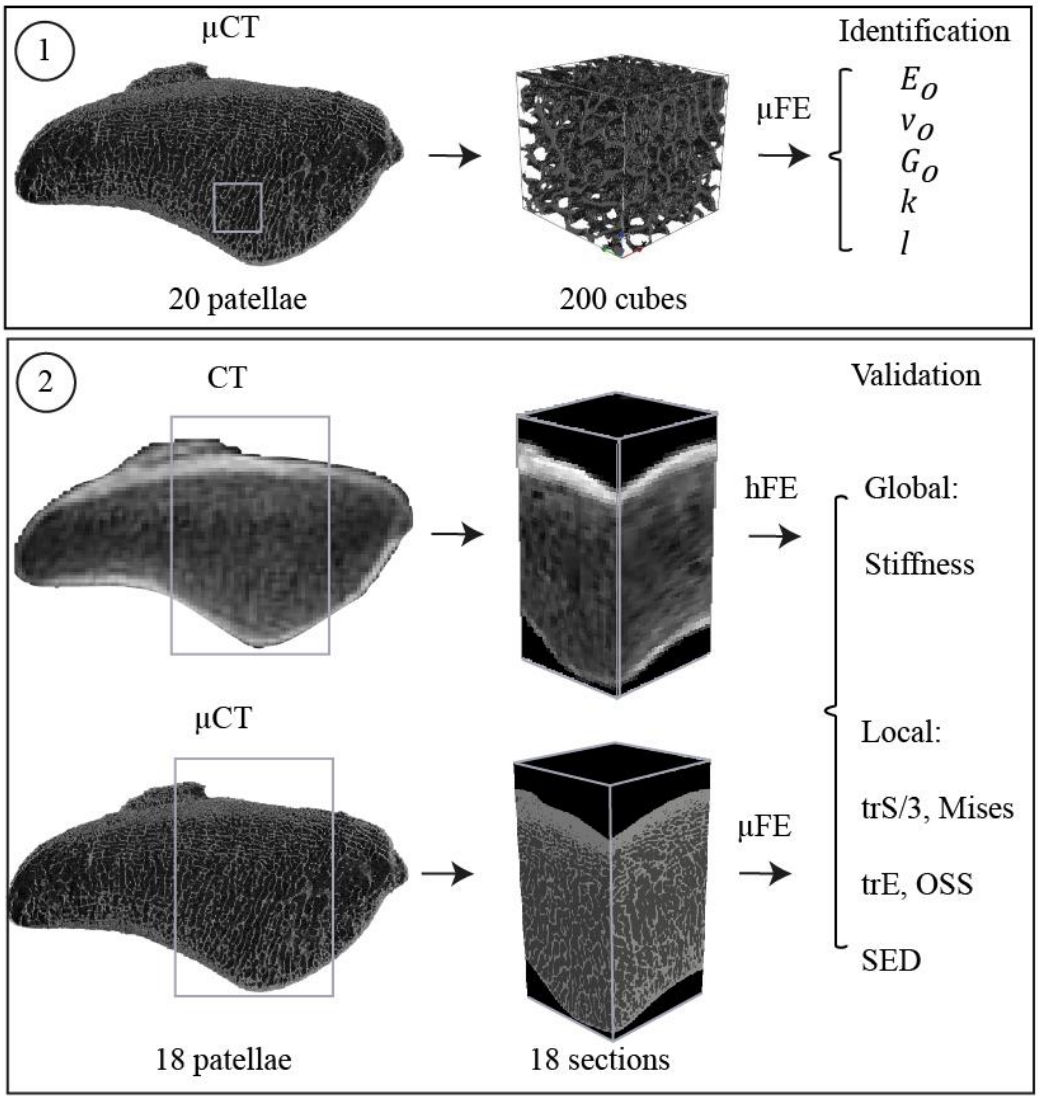

Figure 1. Workflow of the study. The isotropic and anisotropic elastic laws for trabecular bone based on bone volume fraction and fabric anisotropy were identified via µFE for 200 cubic specimens (1). Those material models were validated against µFE by comparing the stiffness and local strain and stress measures (volumetric strain (trE) and stress (trS/3), octahedral shear strain (OctSS), von Mises stress (Mises) and strain energy density (SED)) of 18 patellar sections (2).

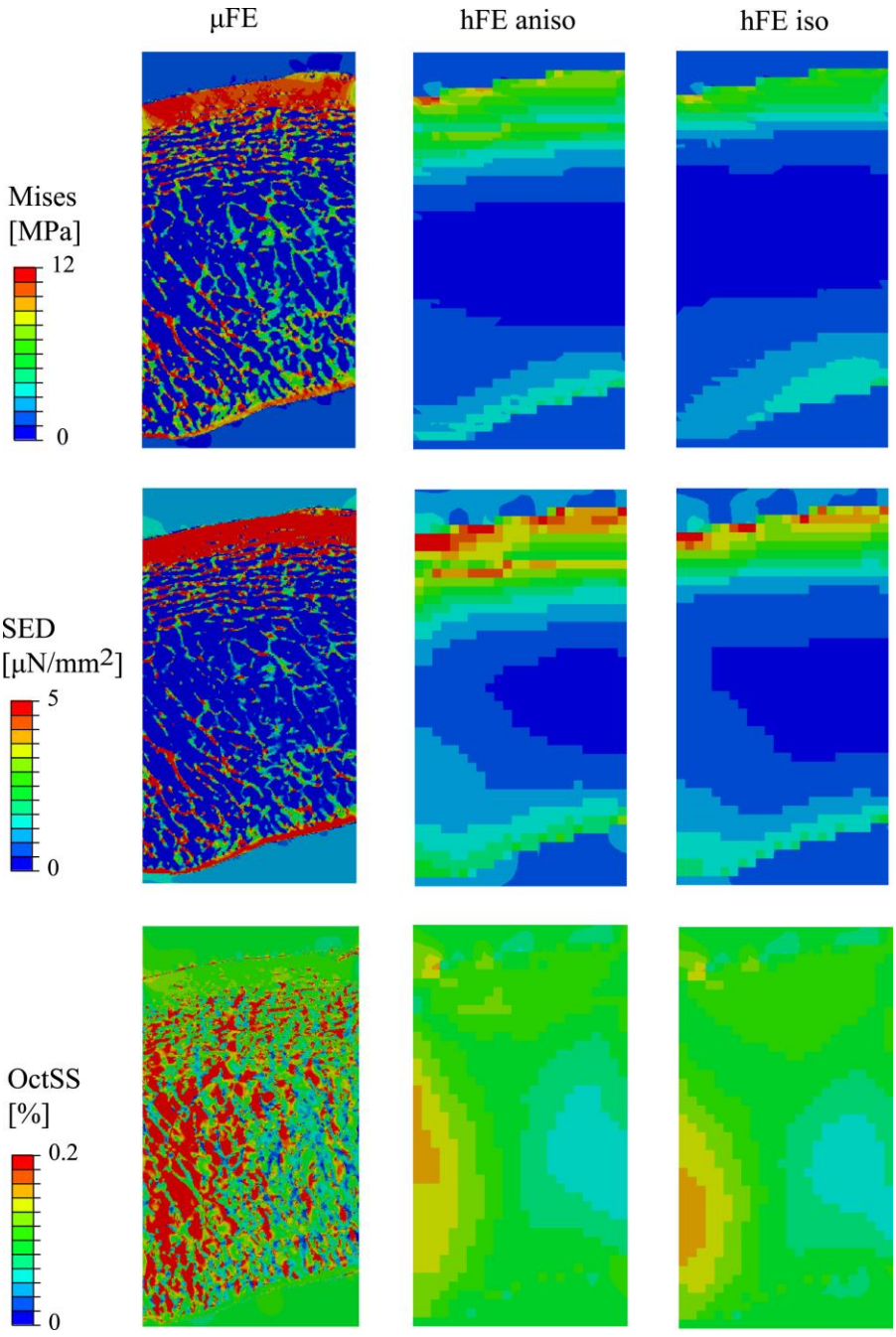

Figure 2. Comparison of von Mises stress (Mises), strain energy density (SED) and octahedral shear strain (OctSS) contour plots of µFE and hFE predictions for the patella under tension in superior-inferior direction (patellar cut in sagittal plane).